Article:
Kesserwani, G. (2013) Topography discretization techniques for Godunov-type shallow water numerical models: a comparative study. Journal of Hydraulic Research , 51 (4). pp. 351-367. ISSN 0022-1686

https://doi.org/10.1080/00221686.2013.796574

Topography discretization techniques for Godunov-type shallow water numerical models: a comparative study

GEORGES KESSERWANI, Department of Civil and Structural Engineering, University of Sheffield, Sheffield, UK

Email: g.kesserwani@shef.ac.uk (Corresponding Author)

ABSTRACT

This paper compares various topography discretization approaches for Godunov-type shallow water numerical models. Many different approaches have emerged popular with Godunov-type water wave models. To date, literature lacks an investigative study distinguishing their pros and the cons, and assessing their reliability relating to issues of practical interest. To address this gap, this work reviews and assesses five standard topography discretization methods that consist of the **Upwind**, the surface gradient method (**SGM**), the mathematically balanced set of the SWE (**Etta-SWE**), the hydrostatic reconstruction technique (**Hydr-Rec**) and the **RKDG2** model. The study further considers mix-mode approaches that incorporate wetting and drying together with the topography discretization. Steady and transient hydraulic tests are employed to measure the performance of the approaches relating to the issues of mesh size, topography's differentiability, accuracy-order of the numerical scheme, and impact of wetting and drying.

Keywords: Godunov-type schemes, topography discretization methods, comparisons, wetting and drying, steady and transient flows.

Preprint submitted to the Journal of Hydraulic Research

Date of submission: 07 April 2013

1. Introduction

Godunov-type shallow water models are featured with the inherent ability to accommodate complex flow transitions within the numerical solution (Toro 2001, Guinot 2003, Toro and García-Navarro 2007). In recent years, they have received applied improvements and have been incorporated into water industry standard software (Lhomme et al. 2010), and used to support flood risk management (Néelz and Pender 2010). In this context, applicable Godunov-type water wave models are at most second-order accurate and require a topography discretization technique and a wetting and drying condition (see Delis and Kampanis 2009 for a comprehensive review).

In its simplistic view, a Godunov-type scheme provides a first-order accurate model that is conceptually based (Godunov 1959). It employs the Finite Volume (FV) framework to approximate the integral of the flow variables – relative to the shallow water equations (SWE) cast in a conservative form – as piecewise-constant per local discrete element but with inter-elemental discontinuities; these discontinuities are combined via the solution of the Riemann problem to provide a sound approximation to the inter-elemental fluxes (Toro 2001). To achieve a second-order accurate formulation in a Godunov-type framework, the MUSCL interpolation approach is often employed (Van Leer 1979), which rests on (extrinsic) reconstruction of piecewise-linear solutions from the initial local piecewise-constant data. However, the MUSCL method compromises with larger and non-local calculation stencils. More recently, with the establishment of the discontinuous Galerkin (DG), a local second-order (or higher-order) accurate Godunov-type formulation may be intrinsically derived from the conservation laws of the SWE, providing a more sophisticated formulation than the traditional FV framework (Kesserwani and Liang 2011).

The incorporation of a topography discretization technique with Godunov-type SWE numerical solvers has been an issue of extreme relevance to their practical development. In respect of this, various discretization approaches have appeared, over the last two decades, which are featured with the ability to maintain a correct discrete balance between topography gradient and the spatial flux. Such a numerical model has been referred to be "*well-balanced*" or to satisfy the "C-property" (Bermúdez and Vázquez-Cendón 1994, Greenberg and LeRoux 1996, LeVeque 1998). Among the popular topography discretization approaches, the sophisticated **Upwind** approach is the eldest. It was derived by Bermúdez and Vázquez-Cendón (1994) for a first-order accurate formulation and was then adopted to integrate the topography within higher-order FV-based Godunov-type models (e.g. García-Navarro and Vázquez-Cendón 1999, Vulovic and Sopta 2002, Crnjaric-Zic et al. 2004). However, the Upwind approach is renowned for its complexity in implementation and its limitation to a FV approximation (Zhou et al. 2001, Kesserwani et al. 2010). The Surface Gradient Method (**SGM**) relies on numerical reconstruction to the free-surface elevation and discretises the

topography source term using a cell-centred pointwise approach. It was first reported in Nujic (1995) for a first-order Godunov-type model, and formally formulated in Zhou et al. (2001) for a second-order MUSCL scheme. Alternatively, Rogers et al. (2003) approached the SGM mathematically providing a new well-balanced set for the SWE (referred hereafter to **Etta-SWE**) that incorporates the free-surface elevation as a main flow variable, and with which the topography source term discretizes in pointwise manner. The Etta-SWE approach was further improved and verified for a MUSCL second-order scheme in the work of Liang and Borthwick (2009). Another popular approach for constructing well-balanced shallow water numerical model is the one established by Audusse et al. (2004), which is known as the hydrostatic reconstruction approach (referred hereafter to **Hydr-Rec**). The Hydr-Rec method reconstructs the free-surface elevation – likewise to the SGM – but acts differently to balance the flux and topography gradients so that to further maintain the positivity of the water depth, and as such provides the further ability to cope with wetting and drying. The Hydr-Rec approach has been successfully applied– as a topography discretization technique – to various high-order Godunov-type models such as WENO-FV and DG methods (Xing and Shu 2006, Noelle et al. 2007), and further enhanced – as a wetting and drying condition – with both FV and DG second-order Godunov-type models (Liang 2010, Kesserwani and Liang 2012). As to the DG method, Xing and Shu (2006) demonstrated theoretically that it is by far the simplest approach to obtain the well-balanced shallow water numerical model. In light of this, Kesserwani et al. (2010) devised a second-order Runge-Kutta DG method (RKDG2) that is effortlessly well-balanced in which the local discrete topography is taken as piecewise-linear but globally continuous. This topography setting is particular to the **RKDG2** framework which is experienced to be more costly than FV-based Godunov-type model. Unquestionably, this review is far from being complete and has only focused on the topography discretization approaches that will serve the purpose of this investigation. Nonetheless, for a more detailed review including the latest trends on the topic of source terms discretization within Godunov-type models, the reader is referred, for instance, to the work of George (2008), LeFloch and Tanh (2011), and Murillo and García-Navarro (2010, 2012).

Despite the notable progress in the design of topography discretization techniques, literature, to date, lacks a study comparing between techniques that are commonly used within Godunov-type shallow water models. From this perspective, the aim of this article to diagnostically compare popular topography discretization techniques used within Godunov-type numerical flow solvers. The selected candidates mainly consists of the five techniques reviewed above; this study attempts to reveal their pros and cons while addressing questions that are believed to be of interest to hydraulic modellers, software developers and potential practitioners; these questions include:

(i) To what extent of mesh-resolution and/or problem's complexity each of the currently existing topography discretization methods is reliably applicable?

(ii) What is the topography discretization technique that provides the best trade-off between accuracy, efficiency, robustness for wider range of applications?

The study namely focuses on the Upwind, SGM, Etta-SWE and Hydr-Rec approaches taken, respectively, with first- and second-order FV formulations, the RKDG2 second-order formulation and combined approaches incorporating the Hydr-Rec within the different second-order formulations. Herein, the key ingredient of each of the selected approaches will be described, and a total of seven approaches will be investigated using various hydraulic test cases with increasing level of complexity. The performance of each approach will be explored and discussed in light of the questions **(i)** and **(ii)**, and relating to effect of wetting and drying. Finally, findings will be summarized and key-conclusions will be drawn.

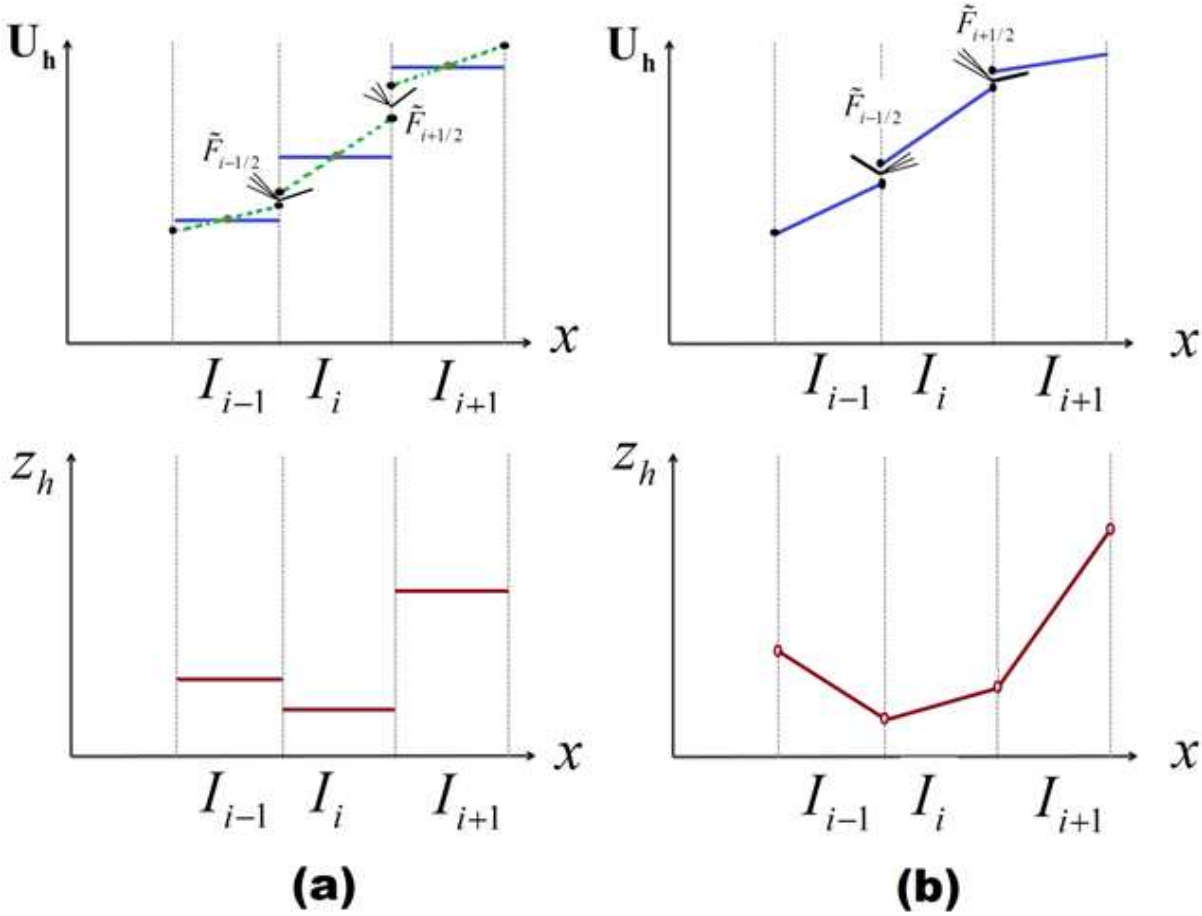

Figure 1. *Local* discretization of flow and topography data: (a) FV method using piecewise-constant data, and with which MUSCL interpolation maybe (extrinsically) applied to produce piecewise-linear reconstructions; (b) DG2 evolution data that are inherently piecewise-linear.

2. Depth-averaged Shallow Water Equations (SWE)

From the principles of mass and momentum conservation, the 1D mathematical model of the SWE can be cast in a conservative matrix form:

$$\partial_t \mathbf{U} + \partial_x \mathbf{F}(\mathbf{U}) = \mathbf{S}(\mathbf{U}) \tag{1}$$

In which (x ,t) are the space-time coordinates. **U** is the vector of the conserved quantities or of flow variables, **F(U)** is the flux vector and **S**(**U**) is the vector containing the topography gradient term:

$$\mathbf{U} = \begin{pmatrix} h \\ q \end{pmatrix},\ \mathbf{F} = \begin{pmatrix} q \\ \dfrac{q^2}{h} + \dfrac{gh^2}{2} \end{pmatrix} \text{ and } \mathbf{S} = \begin{pmatrix} 0 \\ -gh\ \partial_x z \end{pmatrix} \tag{2}$$

Where g (m^2/s) is the constant gravitational acceleration, h (m) is the water depth, $q = hu$ (m^2/s) is the unit-width discharge expressed in terms of the velocity u (m/s). By involving the Jacobian matrix of the flux with respect to the flow vector (**J** = ∂**F**(**U**)/ ∂**U**), the system (1) can be expressed in a quasi-linear form (i.e. $\partial_t \mathbf{U} + \mathbf{J}\partial_x \mathbf{U} = \mathbf{S}$). **J** has two real eigenvalues $\lambda^{1,2} = u \pm c$ (where $c = \sqrt{gh}$ is the wave celerity) and has a complete set of independent real eigenvectors $\mathbf{e}^{1,2} = [1, \lambda^{1,2}]^T$.

3. Godunov-type numerical methods

A 1D computational domain [$x_{\min}$; $x_{\max}$] is subdivided into N uniform cells, via interface points $x_{\min} = x_{1/2} < x_{3/2} \ldots < x_{N+1/2} = x_{\max}$, so that a random cell $I_i = [x_{i-1/2}; x_{i+1/2}]$ is centred at $x_i = 0.5(x_{i-1/2} + x_{i+1/2})$ and of length $\Delta x = x_{i+1/2} - x_{i-1/2}$. In what follow, the local approximate solution of the flow variables will be denoted by $\mathbf{U_h}$ and, consistently, the local approximation of topography function will be denoted by z_h.

3.1. Finite volume (FV) approximation (first- and second- order)

In an FV framework, a Godunov-type transformation to the conservative form (1) represents *locally* the flow variables as piecewise-constant, i.e. $\mathbf{U_h}\,|_{I_i} = \mathbf{U}_i = [h_i;\ q_i]^T$, and likewise for the topography data, i.e. $z_h\,|_{I_i} = z_i$ (see Figure 1a), yielding the semi-discrete formulation below:

$$\frac{d}{dt}\mathbf{U_h}\,|_{I_i} = -\frac{1}{\Delta x}\left(\tilde{\mathbf{F}}_{i+1/2} - \tilde{\mathbf{F}}_{i-1/2}\right) + \mathbf{S_h}\,|_{I_i} \tag{3}$$

The fluxes, e.g. $\tilde{\mathbf{F}}_{i+1/2}$ at the interfaces $x_{i+1/2}$ (shared by adjacent cells I_i and I_{i+1}), are obtained by solving the local Riemann problem according to the approximate solver of Roe (1981):

$$\tilde{\mathbf{F}}_{i+1/2} = \tilde{\mathbf{F}}^{Roe}\left(\mathbf{U}^{-}_{i+1/2}, \mathbf{U}^{+}_{i+1/2}\right) = \frac{1}{2}\left[\mathbf{U}^{-}_{i+1/2} + \mathbf{U}^{+}_{i+1/2} - \sum_{p=1}^{2} \alpha^{p}_{i+1/2} \left|\tilde{\lambda}^{p}_{i+1/2}\right| \tilde{\mathbf{e}}^{p}_{i+1/2}\right] \tag{4}$$

that is supported with the following entropy fix (to reinforce capturing of transcritical flows):

$$\left|\tilde{\lambda}^{p}_{i+1/2}\right|^{*} = \begin{cases} \left|\tilde{\lambda}^{p}_{i+1/2}\right| & \text{if} \quad \left|\tilde{\lambda}^{p}_{i+1/2}\right| \geq \varepsilon^{p}_{i+1/2} \\ \left(\tilde{\lambda}^{p}_{i+1/2}\right)^{2} / (2\varepsilon^{p}) + \varepsilon^{p} / 2 & \text{if} \quad \left|\tilde{\lambda}^{p}_{i+1/2}\right| < \varepsilon^{p}_{i+1/2} \end{cases} \tag{5}$$

$$\text{and } \varepsilon^{p}_{i+1/2} = \min\left\{\tilde{c}_{i+/1/2}, \max\left[0, 2\left(\lambda^{p,+}_{i+1/2} - \lambda^{p,-}_{i+1/2}\right)\right]\right\}$$

The mean eigenvalues $\tilde{\lambda}^{p}_{i+1/2}$, associated eigenvectors $\tilde{\mathbf{e}}^{p}_{i+1/2}$, and p^{th} wave strengths $\alpha^{p}_{i+1/2}$ can be found via explicit formulae involving the Roe averages of the velocity and celerity, and the flow variables involved in $\mathbf{U}^{-}_{i+1/2}$ and $\mathbf{U}^{+}_{i+1/2}$ (Roe 1981); where $\mathbf{U}^{-}_{i+1/2} = \mathbf{U}_{\mathbf{h}}|_{I_i}(x^{-}_{i+1/2})$ and $\mathbf{U}^{+}_{i+1/2} = \mathbf{U}_{\mathbf{h}}|_{I_{i+1}}(x^{+}_{i+1/2})$ denotes the limits of the approximate solution at the interface $x_{i+1/2}$.

To obtain a second-order accurate scheme, these limits are often interpolated using the MUSCL approach for reconstructing piecewise-linear solution from the initial piecewise-local constant approximation (van Leer B, 1979), as shown in Figure 1a:

$$\mathbf{U}^{-}_{i+1/2} = \mathbf{U}_{\mathbf{h}}|_{I_i} + 0.5\nabla_i\left(\mathbf{U}_{\mathbf{h}}\right) \tag{6}$$

$$\mathbf{U}^{+}_{i+1/2} = \mathbf{U}_{\mathbf{h}}|_{I_{i+1}} - 0.5\nabla_{i+1}\left(\mathbf{U}_{\mathbf{h}}\right) \tag{7}$$

Where
$$\nabla_i\left(\mathbf{U}_{\mathbf{h}}\right) = \boldsymbol{\varphi}\left(\frac{\mathbf{U}_{\mathbf{h}}|_{I_i} - \mathbf{U}_{\mathbf{h}}|_{I_{i-1}}}{\mathbf{U}_{\mathbf{h}}|_{I_{i+1}} - \mathbf{U}_{\mathbf{h}}|_{I_i}}\right)\left(\mathbf{U}_{\mathbf{h}}|_{I_i} - \mathbf{U}_{\mathbf{h}}|_{I_{i-1}}\right) \tag{8}$$

$\boldsymbol{\varphi}(\mathbf{r}) = \max\left[0, \min(1, \mathbf{r})\right]$ is the *minmod* limiter that controls the variation of the slope components to avoid spurious oscillations that would possibly occur around discontinuities (Toro 2001). Finally, time-discretization in (3) is achieved using the explicit two-stage Runge-Kutta (RK) time stepping controlled by the Courant-Friedrich-Lewy (CFL) condition with a CFL number equal to 0.75.

Alternatively, to obtain a first-order scheme, it suffice to: (a) zero the gradient terms within (6) and (7), i.e. $\mathbf{U}^{-}_{i+1/2} = \mathbf{U}_{\mathbf{h}}|_{I_i}$ and $\mathbf{U}^{+}_{i+1/2} = \mathbf{U}_{\mathbf{h}}|_{I_{i+1}}$, and (b) use only the first stage of the RK discretization to lift the solution to the next time level.

3.2. Discontinuous Galerkin (DG) spatial approximation (second-order)

The DG method conceptually extends the local FV interpretation to higher than first-order accuracy by integrating the Finite Element (FE) notion. The DG method is locally conservative and allows scaling in accuracy (Cockburn and Shu 2001). For a 1D second-order

DG discretisation (DG2), the sough solution is locally piecewise-linear (i.e. Figure 1b) and is spanned by two time-evolving FE coefficients, i.e. $\mathbf{U_h}|_{I_i} = \left\{\mathbf{U}_i^0, \mathbf{U}_i^1\right\}$. It expands locally as:

$$\mathbf{U_h}\left(x,t\right)\Big|_{I_i} = \mathbf{U}_i^0(t) + \mathbf{U}_i^1(t)\frac{\left(x-x_i\right)}{\Delta x/2} \qquad \left(\forall x \in I_i\right) \tag{9}$$

The semi-discrete local transformation of the conservative form (1) now produces two spatial operators for the update of the two local FE coefficients, respectively:

$$\frac{d}{dt}\begin{pmatrix} \mathbf{U}_i^0(t) & 0 \\ 0 & \mathbf{U}_i^1(t) \end{pmatrix} = \begin{pmatrix} \mathbf{L}_i^0 & 0 \\ 0 & \mathbf{L}_i^1 \end{pmatrix} \tag{10}$$

Where $\mathbf{L}_i^0$ and $\mathbf{L}_i^1$ are the DG2 local discrete representation to the flux and source terms vectors in (1), which can be manipulated to give (Kesserwani and Liang 2011):

$$\mathbf{L}_i^0 = -\frac{1}{\Delta x}\left(\tilde{\mathbf{F}}_{i+1/2} - \tilde{\mathbf{F}}_{i-1/2}\right) + \mathbf{S_h}|_{I_i} \tag{11}$$

$$\begin{aligned}\mathbf{L}_i^1 = -\frac{3}{\Delta x}\Big\{ & \tilde{\mathbf{F}}_{i+1/2} + \tilde{\mathbf{F}}_{i-1/2} - \mathbf{F}|_{I_i}\left(\mathbf{U}_i^0 + \mathbf{U}_i^1/\sqrt{3}\right) - \mathbf{F}|_{I_i}\left(\mathbf{U}_i^0 - \mathbf{U}_i^1/\sqrt{3}\right) \\ & - \frac{\Delta x\sqrt{3}}{6}\left[\mathbf{S_h}|_{I_i}\left(\mathbf{U}_i^0 + \mathbf{U}_i^1/\sqrt{3}\right) - \mathbf{S_h}|_{I_i}\left(\mathbf{U}_i^0 - \mathbf{U}_i^1/\sqrt{3}\right)\right]\Big\}\end{aligned} \tag{12}$$

Similar to the second-order version of the FV method, non-oscillatory solution around sharp gradients is ensured using the *minmod* limiter. However, the DG method further requires restricting the slope limiting process to the so-called troubled-slope components, which have been identified according to the discontinuity detector of Krivodonova et al. (2004). The fluxes, e.g. at the interface $x_{i+1/2}$, are evaluated using the also the Roe Riemann solver (4) and (5), but with a direct involvement of the limits defined by the local piecewise-linear solutions at $x_{i+1/2}$ (see Figure 1b). Finally, each of the local coefficients, $\mathbf{U}_i^0(t)$ and $\mathbf{U}_i^1(t)$, is advanced in time using the explicit double-stage RK time discretization, but with a CFL number equal to 0.3 (Cockburn and Shu 2001).

4. Topography discretization techniques

This section briefly summarises the key ingredient(s) of the topography discretization models that are commonly used within the Godunov-type methods presented in Section 3, and will be compared later in Section 5. The described techniques are all featured by the ability to verify the discrete balance with the flux gradient for unperturbed steady flows (i.e. satisfy the *C*-property or provide a well-balanced scheme).

4.1 Surface Gradient Method (SGM)

The SGM is widely used with FV Godunov-type schemes. It is credited to Zhou et al. (2001) where a theoretical verification of the C-property is available. Within the scheme (3)-(8) the operation of the SGM may be summarized as:

1. Reconstruct ($h + z = \eta$) limits at interface $x_{i+1/2}$ from the variable h and the topography z: $\eta^{-}_{i+1/2} = (h_i + z_i) + 0.5\nabla_i(h+z)$ and $\eta^{+}_{i+1/2} = (h_{i+1} + z_{i+1}) - 0.5\nabla_{i+1}(h+z)$.
2. Evaluate the discharge limits at interface $x_{i+1/2}$: $q^{-}_{i+1/2} = q_i + 0.5\nabla_i(q)$ and $q^{+}_{i+1/2} = q_{i+1} - 0.5\nabla_{i+1}(q)$
3. Set a single topography value at interface $x_{i+1/2}$ defined by the average $z^{\pm}_{i+1/2} = (z^{-}_{i+1/2} + z^{+}_{i+1/2})/2$ where $z^{-}_{i+1/2} = z_i$ and $z^{+}_{i+1/2} = z_{i+1}$.
4. Redefine the Riemann states at $x_{i+1/2}$ according to the averaged topography $z^{\pm}_{i+1/2}$: $h^K_{i+1/2} = \eta^K_{i+1/2} - z^{\pm}_{i+1/2}$ and $u^K_{i+1/2} = q^K_{i+1/2} / h^K_{i+1/2}$ (where $K = +, -$). From these, calculate the flux $\tilde{\mathbf{F}}_{i+1/2}$ using equation (4), in which $\mathbf{U}^K_{i+1/2} = [h^K_{i+1/2}, q^K_{i+1/2}]^T$.
5. Repeat steps 1-4 to further evaluate flux at $\tilde{\mathbf{F}}_{i-1/2}$ interface $x_{i\text{-}1/2}$.
6. Set $\overline{h} = (h^{-}_{i+1/2} + h^{+}_{i-1/2})/2$ and $\partial_x z = (z^{\pm}_{i+1/2} - z^{\pm}_{i-1/2})/\Delta x$ and use them to evaluate $\mathbf{S}_{\mathbf{h}}|_{I_i}$ in (3).

4.2 *Mathematically balanced set of SWE (Etta-SWE)*

Initially developed by Rogers et al. (2003) where all derivation details are presented. The Etta-SWE uses an alternative mathematical form of the SWE, in which the free-surface elevation η becomes the main flow variable, instead of h, so as to mathematically verify the C-property (Liang and Borthwick 2009). With this change of variables, the conservative vectorial form (1) is described according to the expressions below:

$$\mathbf{U} = \begin{pmatrix} \eta \\ q \end{pmatrix},\ \mathbf{F} = \begin{pmatrix} q \\ \dfrac{q^2}{\eta - z} + \dfrac{g}{2}(\eta^2 - 2\eta z) \end{pmatrix} \text{ and } \mathbf{S} = \begin{pmatrix} 0 \\ -g\eta\ \partial_x z \end{pmatrix} \tag{13}$$

For the scheme (3)-(8) the key-steps of the Etta-SWE may be summarized as:

1. Directly evaluate η limits at interface $x_{i+1/2}$: $\eta^{-}_{i+1/2} = \eta_i + 0.5\nabla_i(\eta)$ and $\eta^{+}_{ii+1/2} = \eta_{i+1} - 0.5\nabla_{i+1}(\eta)$
2. Evaluate the discharge limits at interface $x_{i+1/2}$: $q^{-}_{i+1/2} = q_i + 0.5\nabla_i(q)$ and $q^{+}_{i+1/2} = q_{i+1} - 0.5\nabla_{i+1}(q)$
3. Repeat the steps 3-5 of the SGM.
4. Set $\overline{\eta} = (\eta^{-}_{i+1/2} + \eta^{+}_{i-1/2})/2$ and $\partial_x z = (z^{\pm}_{i+1/2} - z^{\pm}_{i-1/2})/\Delta x$, and evaluate $\mathbf{S}_{\mathbf{h}}|_{I_i}$ in (3).

4.3 *Hydrostatic reconstruction approach (Hydr-Rec)*

Established by Audusse et al. (2004) and can further account for wet/dry fronts. Within the scheme (3)-(8), the contribution of the Hydr-Rec may be described as follows:

1. Reconstruct ($h + z = \eta$) and evaluate the discharge limits at interface $x_{i+1/2}$, i.e. do steps 1 and 2 of the SGM.
2. Record velocities at $x_{i+1/2}$ obtained from the original topography data (i.e. $z^{-}_{i+1/2} = z_i$ and $z^{+}_{i+1/2} = z_{i+1}$): $h^K_{i+1/2} = \eta^K_{i+1/2} - z^K_{i+1/2}$ and $u^K_{i+1/2} = q^K_{i+1/2} / h^K_{i+1/2}$; (where $K = +, -$).
3. Topography discretization at interface $x_{i+1/2}$ with wetting and drying:
   a) Re-define *numerically* $z^{K,*}_{i+1/2} = \eta^K_{i+1/2} - h^K_{i+1/2}$, (where $K = +, -$).
   b) Set a single z-value at $x_{i+1/2}$ defined by the maximum, i.e. $z^{\pm,*}_{i+1/2} = \max(z^{-,*}_{i+1/2}, z^{+,*}_{i+1/2})$.
   c) Preserve positivity of water at $x_{i+1/2}$, i.e. $h^{K,*}_{i+1/2} = \max\left(0, \eta^K_{i+1/2} - z^{\pm,*}_{i+1/2}\right)$, ($K = +, -$).
   d) Find discharges incorporating the original velocities, i.e. $q^{K,*}_{i+1/2} = h^{K,*}_{i+1/2}\ u^K_{i+1/2}$, and the free-surface elevations at $x_{i+1/2}$, i.e. $\eta^{K,*}_{i+1/2} = h^{K,*}_{i+1/2} + z^{\pm,*}_{i+1/2}$, associated to the positivity-preserving water depth the single value of the topography.
   e) Ensure that step d) do not possibly cancel the actual water level at a wet/dry front, i.e.
      i. Calculate $\Delta\eta_{i+1/2} = \max\left[0, -\left(\eta^K_{i+1/2} - z^{\pm,*}_{i+1/2}\right)\right]$, i.e. after Step 3-b).
      ii. Adjust $\eta^{K,*}_{i+1/2} \leftarrow \eta^{K,*}_{i+1/2} - \Delta\eta_{i+1/2}$ and $z^{\pm,*}_{i+1/2} \leftarrow z^{\pm,*}_{i+1/2} - \Delta\eta_{i+1/2}$.
4. Find the flux $\tilde{\mathbf{F}}_{i+1/2}$ using $h^{K,*}_{i+1/2} = \eta^{K,*}_{i+1/2} - z^{\pm,*}_{i+1/2}$, and $u^K_{i+1/2} = q^{K,*}_{i+1/2} / h^{K,*}_{i+1/2}$ (after step 3).
5. Repeat steps 1-4 to evaluate flux at $\tilde{\mathbf{F}}_{i-1/2}$ interface $x_{i\text{-}1/2}$.
6. Set $\overline{h} = (h^{-,*}_{i+1/2} + h^{+,*}_{i-1/2})/2$ and $\partial_x z = (z^{\pm,*}_{i+1/2} - z^{\pm,*}_{i-1/2})/\Delta x$, and use them to evaluate $\mathbf{S}_{\mathbf{h}}|_{I_i}$ in (3).

4.4 *Upwind decomposition (Upwind)*

Developed by Bermúdez and Vázquez-Cendón (1994) and is more sophisticated than the others. The Upwind approach projects, or decomposes, the source terms vector **S** onto the characteristic basis using the parameters involved within the Roe flux upwinding (4). The Upwind discretization is theoretically able to maintain the discrete balance among flux gradients and the topography gradient; for instance see within Vázquez-Cendón (1999), García-Navarro and Vázquez-Cendón (2000) for a demonstration of the C-property.

- For the first-order version of scheme (3)-(8), the involvement of the Upwind approach may be briefly expressed as:

$$\mathbf{S_h}\,|_{I_i} = \frac{1}{2}\left[\left(I+|\,\tilde{J}_{i-1/2}\,|\,\tilde{J}_{i-1/2}^{-1}\right)\mathbf{S}_{i-1/2} + \left(I-|\,\tilde{J}_{i+1/2}\,|\,\tilde{J}_{i+1/2}^{-1}\right)\mathbf{S}_{i+1/2}\right] \tag{14}$$

where,

$$\tilde{J}_{i\pm1/2} = \mathbf{R}_{i\pm1/2}\begin{pmatrix}\tilde{\lambda}^1_{i+1/2} & 0\\ 0 & \tilde{\lambda}^2_{i+1/2}\end{pmatrix}\mathbf{R}^{-1}_{i\pm1/2} \text{ and } \mathbf{R}_{i+1/2} = \begin{pmatrix}\tilde{\mathbf{e}}^1_{i+1/2} & \tilde{\mathbf{e}}^2_{i+1/2}\end{pmatrix} = \begin{pmatrix}1 & 1\\ \tilde{\lambda}^1_{i+1/2} & \tilde{\lambda}^2_{i+1/2}\end{pmatrix} \tag{15}$$

and,

$$\mathbf{S}_{i+1/2} = \begin{pmatrix}0\\ -g\left(\frac{h_i+h_{i+1}}{2}\right)\left(\frac{z_{i+1}-z_i}{\Delta x}\right)\end{pmatrix} \text{ and } \mathbf{S}_{i-1/2} = \begin{pmatrix}0\\ -g\left(\frac{h_i+h_{i-1}}{2}\right)\left(\frac{z_i-z_{i-1}}{\Delta x}\right)\end{pmatrix} \tag{16}$$

- For a MUSCL second-order scheme (3)-(8), the Upwind approach also applies but requires a preliminary incorporation of the SGM (i.e. Step 1) to soften the free-surface gradients prior to the action of the slope-limiter (to ultimately produce reliable water depth limits at the interfaces)

4.5 *Local P^1-topography projection within the RKDG2 framework (RKDG2)*

In DG methods, the well-balanced property can be genuinely obtained by projecting the topography function onto the same space of local polynomial approximation (Xing and Shu 2006). For the DG2 setting, the local P^1-topography projection reads (Kesserwani et al. 2010):

$$z_h(x)\big|_{I_i} = z_i^0 + z_i^1\frac{(x-x_i)}{\Delta x/2} \qquad (\forall x \in I_i) \tag{17}$$

$$z_i^0 = \int_{x_{i-1/2}}^{x_{i+1/2}} z(x)\,dx \approx \frac{z(x_{i+1/2})+z(x_{i-1/2})}{2} \tag{18}$$

$$z_i^1 = \int_{x_{i-1/2}}^{x_{i+1/2}} \left(\frac{x-x_i}{\Delta x}\right) z(x)\,dx \approx \frac{z(x_{i+1/2})-z(x_{i-1/2})}{2} \tag{19}$$

The local approximation of the topography gradient expresses as:

$$\partial_x\, z_h(x)\big|_{I_i} = \partial_x\left[z_i^0 + z_i^1\frac{(x-x_i)}{\Delta x/2}\right] = \frac{z_i^1}{\Delta x/2} = \frac{z(x_{i+1/2})-z(x_{i-1/2})}{\Delta x} \tag{20}$$

And the continuity property holds across the entire domain, namely at the interface $x_{i+1/2}$:

$$z_h(x_{i+1/2}^-)\,|_{I_i} = z_i^0 + z_i^1 = z(x_{i+1/2}) = z_{i+1}^0 - z_{i+1}^1 = z_h(x_{i+1/2}^+)\,|_{I_{i+1}} \tag{21}$$

The local RKDG2 method taken with the P^1-projection of the topography verifies exactly the C-property (Kesserwani and Liang 2011).

4.6 *Some relevant mix-mode approaches*

Among the possible blends, it is strategic to look at mix-mode approaches incorporating the Hydr-Rec approach owing to its merit for representing wetting and drying. Therefore, the foreseeable mix-mode approaches for possible study are:

- *Etta-SWE & Hydr-Rec.* Applies the Hydr-Rec after steps 1 and 2 of the Etta-SWE. It may be used to integrate wetting and drying into a shallow water model based on the Etta-SWE model (Liang 2010, Wang et al. 2011).
- *RKDG2 & Hydr-Rec.* Applies the Hydr-Rec with the local RKDG2 solution to the traditional SWE and the local P^1-projection of the topography. However, it requires local incorporation of the free-surface gradients to stabilize the slope-limiting process (Xing and Shu 2006, Kesserwani et al. 2010).
- *Etta-SWE & RKDG2 & Hydr-Rec.* Applies the RKDG2 & Hydr-Rec using the Etta-SWE, which, in effect, implicitly stabilizes the slope-limiting process (Kesserwani and Liang 2012). In terms of performance, this merge is equivalent to the RKDG2 & Hydr-Rec merge, and hence will not be further investigated in this work.
- *Upwind & Hydr-Rec.* This merge does not seem to be directly applicable as the Upwind approach requires keeping the original discontinuous topography limits at interfaces, whereas the Hydr-Rec, contradictorily, needs to impose a single continuous topography value of these two limits. Therefore, this prospective merge will not be further investigated in this work.

Table 1. Verification of the C-property (i.e. $h + z$ = 6m and q = 0) for the case of the *differentiable* topography (22); relative L^2-errors (Er.) and CPU times produced by the ***second-order*** Godunov-type models.

	***N* = 11 (coarse)**			***N* = 21 (medium)**			***N* = 41 (fine)**		
	Er. *h*	**Er. *q***	**CPU**	**Er. *h***	**Er. *q***	**CPU**	**Er. *h***	**Er. *q***	**CPU**
Etta-SWE	1.0e-18	1.2e-15	2.2s	3.4e-18	6.9e-15	8.2s	2.5e-18	2.3e-15	32.2s
Hydr-Rec	1.8e-17	5.1e-15	2.3s	5.5e-18	8.4e-16	7.5s	2.5e-18	1.1e-15	28.2s
SGM	4.0e-18	1.1e-15	2.2s	4.0e-18	3.0e-15	7.9s	2.1e-18	1.3e-15	31.3s
Upwind	4.0e-18	1.7e-15	2.2s	5.1e-18	1.0e-15	8.2s	1.5e-18	1.5e-15	30.6s
RKDG2	3.3e-17	3.7e-14	11s	2.5e-17	3.0e-14	38.5s	7.0e-17	3.4e-14	151s

5. Results and comparisons

This section assesses and compares the FV-based topography discretization techniques (i.e. SGM, Etta-SWE, Hydr-Rec and Upwind), the RKDG2 method and two of the mix-mode methods (i.e. Etta-SWE & Hydr-Rec and RKDG2 & Hydr-Rec). The FV-based approaches

are implemented with the first-order and the second-order Godunov-type model; whereas the mix-mode approaches are only considered with the second-order version. Steady analytical tests are selected to numerically verify the C-property (i.e. $h + z = constant$ and $q = 0$) and to benchmark the models' performance for more complex steady flows (i.e. $\partial_t h = 0$ and $q = constant \neq 0$). Unsteady dam-break flows over steps are introduced to elaborate further on the models' behaviour for conceivable challenging flow scenarios. These particular tests are mainly distinguished by the property of *differentiability* for the topography and the flow. Several mesh sizes are used during the simulations and the relative L^2-Errors with respect to analytical solutions are measured (when applicable) and listed in Tables together CPU runtime costs.

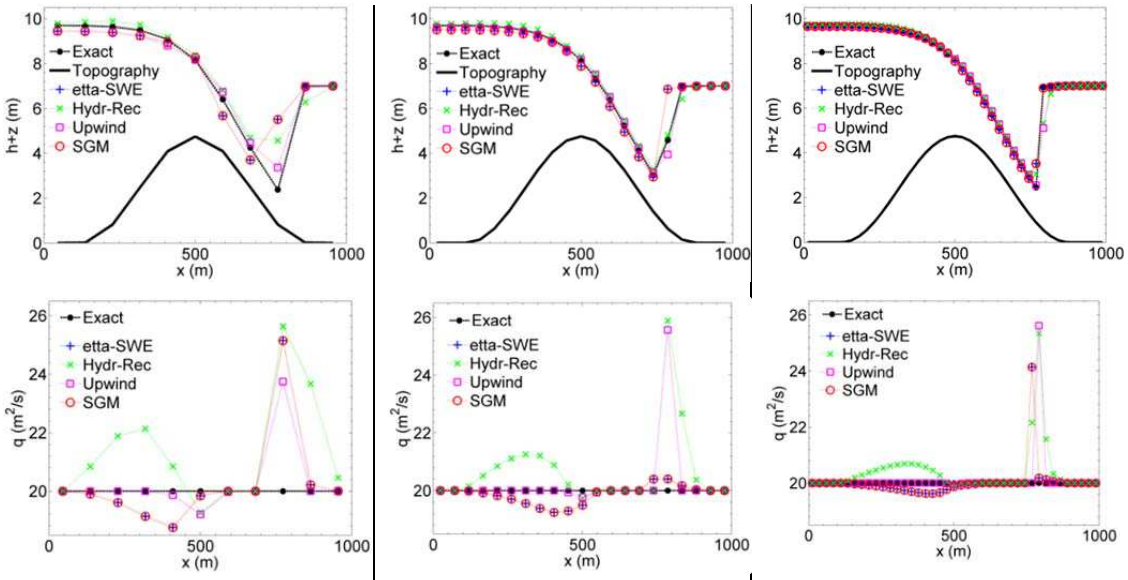

Figure 2. Comparison between the topography discretization models for the ***first-order*** FV schemes; steady flow over *differentiable* topography: (a) $N = 11$, (b) $N = 21$, and (c) $N = 41$.

5.1 *Steady flows over a differentiable topography*

Two steady flow sub-cases are considered; the first for verifying numerically the *C*-property and the second for assessing the ability to simulate flow with non-zero velocity. The channel is 1000m long and the topography is featured by the *differentiability* property and follows a hump-shape between $x = 125$m and $x = 875$m, i.e.

$$z(x) = 4.75 sin^2\left(\frac{x-125}{750}\pi\right) \tag{22}$$

For the first sub-case, the initial conditions are $h + z = 6$m and $q = 0$ m^2/s with no external disturbance imposed during the simulations. Therefore the initial state should be maintained if the numerical model balances properly the flux gradient with the topography gradient. Since this is a still water test, the boundary condition (numerical) can be either

transmissive or reflective and do not affect the predictions. A series of simulations is carried out on computational grids with N = 11, 21, 41 cells, respectively, and up to t = 2000s. The relative L^2-errors for the water depths and the discharges produced by the second-order Godunov-type models are listed in Table 1. The errors are in the range of machine precision and hence confirm that all the considered topography discretization techniques are able to balance the numerical flux with topography gradient for a *differentiable* topography.

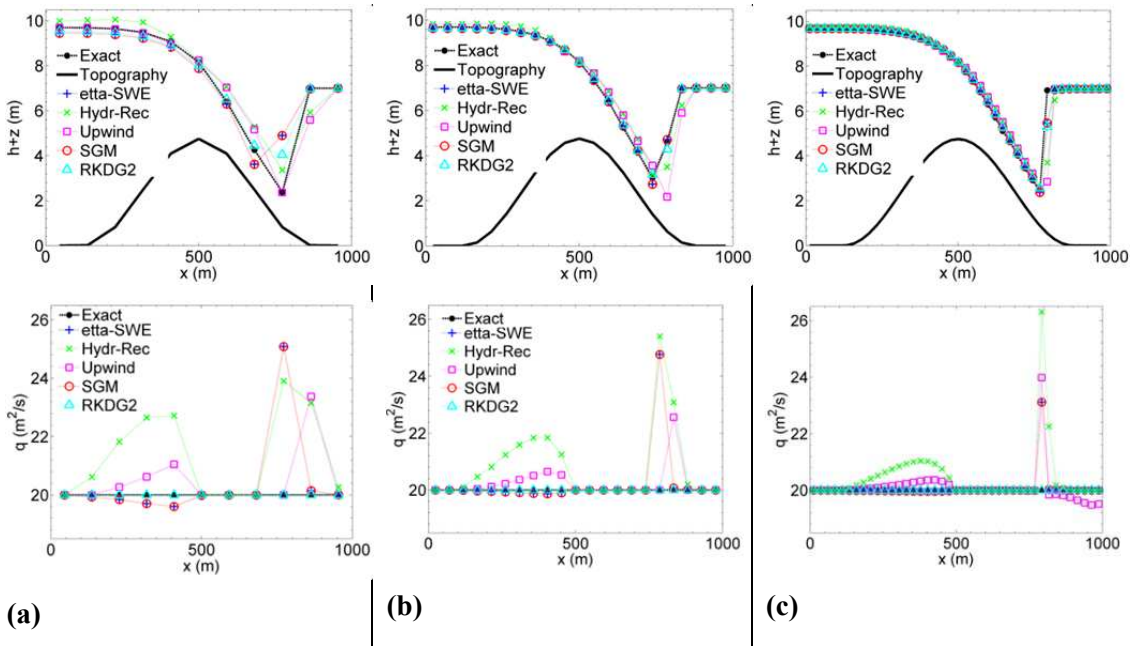

Figure 3. Comparison between the topography discretization models for the ***second-order*** Godunov-type schemes; steady flow over *differentiable* topography: (a) N = 11, (b) N = 21, and (c) N = 41.

For the second sub-case, a steady flow with moving water is assumed whereby the flow undergoes a transcritical flow transition at the middle of the channel and a hydraulic jump downstream of the hump. A steady inflow boundary condition of 20m^2/s is imposed and the outflow boundary is a water level of 7m. A simulation starts from an initial water height of 8m, and stops after a relatively long time evolution (i.e. t = 2000s). Sets of simulations are run, on the same meshes as before, and using the first- and second-order Godunov-type schemes, respectively. Figure 2 and Figure 3 present the respective predictions, where the numerical depths and discharges realized by the different topography discretization methods are compared with the analytical depth and discharge. The associated relative L^2-errors are listed in Table 2 and Table 3, respectively.

In the ***first-order*** model, as shown in Figure 2 and Table 2, the Upwind approach outperform the other approaches for all meshes; for the coarsest and medium meshes, its relative errors are noted to be one order of magnitude less than for the other techniques. The

Etta-SWE and the SGM are seen to produce similar outcomes (quantitative and qualitative) with an under-estimating tendency that is observed to reduce with the doubling and quadrupling in the mesh density. The Hydr-Rec has generally delivered close performance alike the others but showing a clear trend to over-estimate predictions; its good behaviour is namely noted in the capture of the hydraulic jump where – together with the Upwind – it surpasses the Etta-SWE and the SGM for the coarse and medium meshes.

Table 2. L^2-error (Er.) for flow variables and CPU times produced using the ***first-order scheme*** at t = 2000s; transcritical flow with shock over a *differentiable* topography.

	***N* = 11 (coarse)**			***N* = 21 (medium)**			***N* = 41 (fine)**		
	Er. *h*	**Er. *q***	**CPU**	**Er. *h***	**Er. *q***	**CPU**	**Er. *h***	**Er. *q***	**CPU**
Eta-SWE	1.1e-02	7.4 e-03	2.5s	3.2e-03	8.0e-04	7.8s	5.3e-04	8.0e-04	30.7s
Hydr-Rec	8.8e-02	1.0e-02	1.2s	1.2e-03	3.6e-03	5.3s	8.8e-04	1.2e-03	19.4s
SGM	1.1e-02	7.4e-03	1.9s	3.2e-03	8.4e-04	7.1s	5.3e-04	8.0e-04	23s
Upwind	4.2e-03	5.3e-03	1.3s	2.1e-04	9.7e-04	5.2s	8.8e-04	1.1e-03	20.1s

Table 3. L^2-error (Er.) for flow variables and CPU times produced by the ***second-order schemes*** at t = 2000s; transcritical flow with shock over a differentiable topography.

	***N* = 11 (coarse)**			***N* = 21 (medium)**			***N* = 41 (fine)**		
	Er. *h*	**Er. *q***	**CPU**	**Er. *h***	**Er. *q***	**CPU**	**Er. *h***	**Er. *q***	**CPU**
Etta-SWE	9.3e-03	7.0e-03	6.5s	4.8e-04	2.5e-03	21.4s	7.1e-04	5.9e-04	80.0s
Hydr-Rec	7.2e-03	9.0e-03	4.4s	2.3e-03	3.8e-03	17.0s	1.7e-03	1.4e-03	62.7s
SGM	9.3e-03	7.0e-03	6.4s	4.8e-04	2.5e-03	22.0s	7.1e-04	5.9e-04	71.4s
Upwind	6.3e-03	4.9e-03	5.4s	3.7e-03	1.4e-03	20.2s	2.0e-03	8.0e-04	68.5s
RKDG2	6.0e-03	1.0e-12	25s	5.1e-04	3.2e-13	74.4s	7.9e-04	2.6e-13	316s

With the ***second-order*** accurate models, as illustrates Figure 3 and Table 3, the Hydr-Rec and Upwind are detected to comparatively underperform contrasted against the Etta-SWE and the SGM that are noted to excel with the second-order scheme. For the coarse and medium meshes, the Etta-SWE and the SGM errors – relative to the second-order scheme – are observed to be one order-of-magnitude lower than their errors relative to the first-order model (i.e. Tables 2 vs. Table 3). Moreover, their predictive capability notes drastic improvement with mesh refinement. Consequently, it is worth commenting that among the FV-based topography discretization approaches, the Etta-SWE and the SGM appear to be more

appropriate to the second-order MUSCL scheme. The RKDG2 model could mimic the analytical profiles with an ideal accuracy. Remarkably, its level accuracy is noted to reasonably match the Etta-SWE and SGM on the fine mesh; however in this setting, the RKDG2 approach trades-off with an excessive runtime cost (Table 3). Overall, for steady flow over a *differentiable topography*, all the FV-based topography discretization approaches are applicable on reasonably fine meshes. However, these preliminary results suggest giving preference to Upwind and Hydr-Rec within a first-order scheme and to SGM and Etta-SWE within the second-order MUSCL scheme. The RKDG2 method, although provides the finest capture to flow transition, seems to be opportune for very coarse meshes where its runtime are relatively comparable.

Table 4. Verification of the C-property for a fully wet-domain involving a *non-differentiable* topography; relative L^2-error (Er.) for flow variables and CPU times.

	***N* = 11 (coarse)**			***N* = 21 (medium)**			***N* = 41 (fine)**		
	Er. *h*	**Er. *q***	**CPU**	**Er. *h***	**Er. *q***	**CPU**	**Er. *h***	**Er. *q***	**CPU**
Eta-SWE	5.9e-18	3.3e-14	3.4s	1.0e-17	5.0e-14	12.3s	1.7e-18	1.3e-14	47.3s
Hydr-Rec	9.7e-18	4.0e-15	3.3s	4.0e-18	2.1e-15	12.0s	1.6e-18	3.7e-15	40.7s
SGM	5.7e-18	1.9e-14	3.5s	7.2e-18	5.3e-14	11.5s	2.0e-18	3.0e-15	44.0s
Upwind	5.7e-18	7.8e-15	3.6s	5.9e-18	2.3e-15	12.6s	2.3e-18	2.0e-14	45.2s
RKDG2	4.0e-17	1.8e-14	16.9s	2.6e-17	1.2e-14	56.5s	5.8e-17	5.2e-14	210s

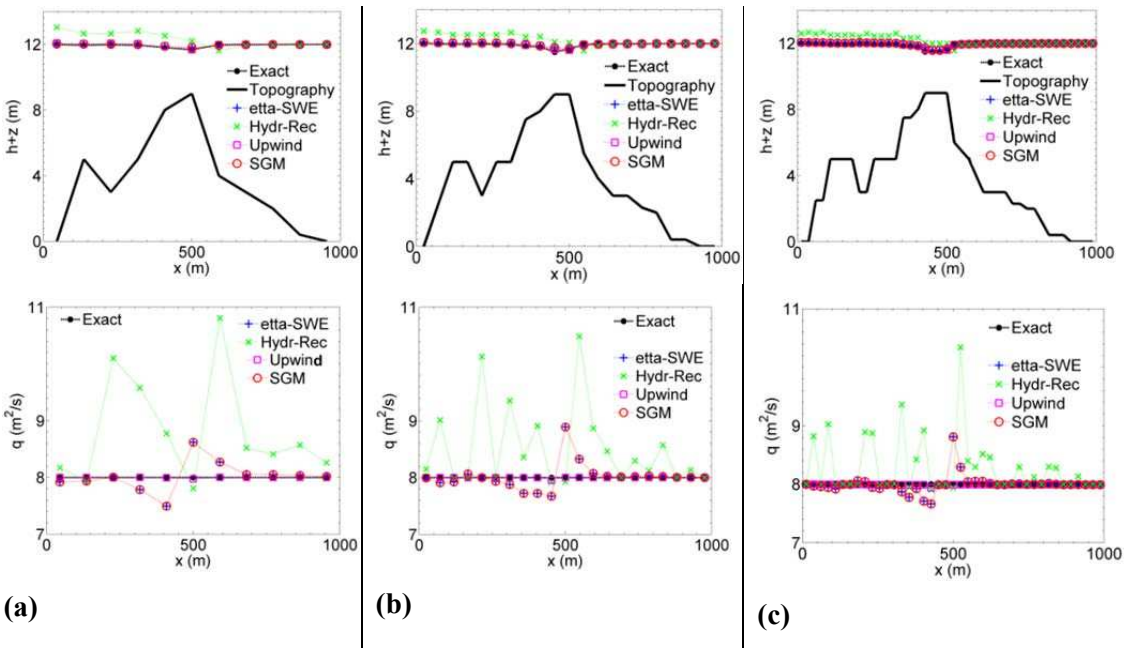

Figure 4. Comparison between the topography discretization approaches for the ***first-order*** FV schemes; steady flow over a *non-differentiable* topography: (a) $N = 11$, (b) $N = 21$, and (c) $N = 41$.

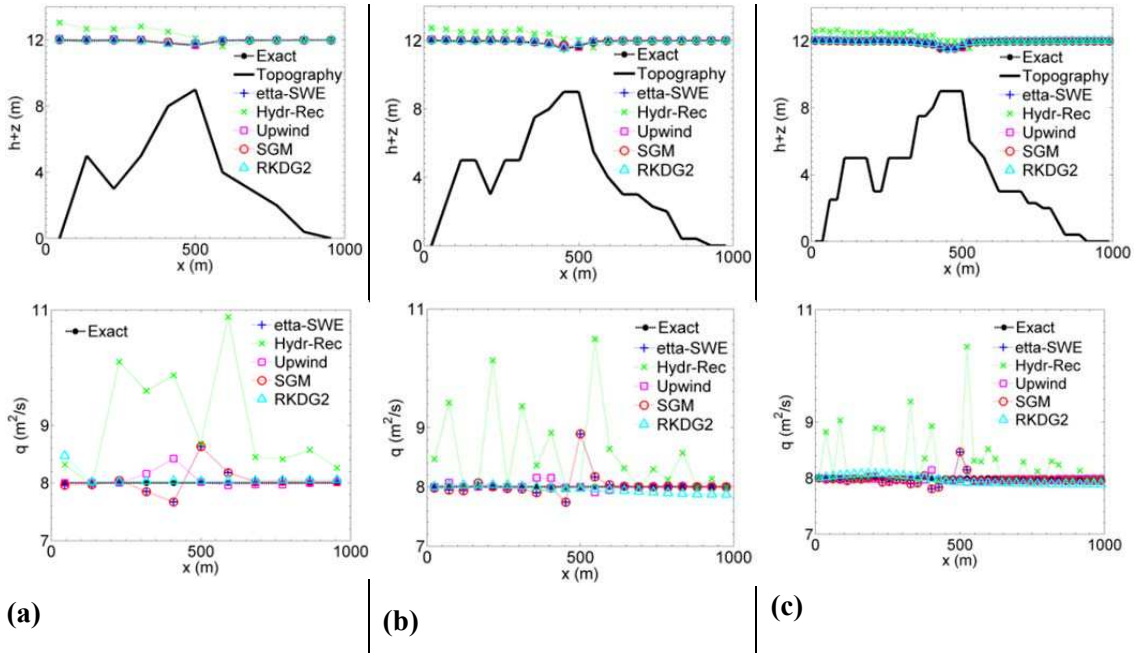

Figure 5. Comparison between the topography discretization approaches for the ***second-order*** Godunov-type schemes; steady flow over a *non-differentiable* topography: (a) $N = 11$, (b) $N = 21$, and (c) $N = 41$.

Table 5. L^2-error (Er.) for flow variables and CPU times produced by the ***first-order FV schemes*** at $t = 2000$s; steady smooth flow over a *non-differentiable* topography.

	***N* = 11 (coarse)**			***N* = 21 (medium)**			***N* = 41 (fine)**		
	Er. *h*	**Er. *q***	**CPU**	**Er. *h***	**Er. *q***	**CPU**	**Er. *h***	**Er. *q***	**CPU**
Eta-SWE	4.1e-04	3.0 e-02	1.4s	2.8e-04	1.4e-03	5.6s	1.1e-04	4.8e-04	21.6s
Hydr-Rec	4.4e-03	1.4e-02	1.2s	1.7e-03	5.2e-03	4.1s	8.0e-04	1.7e-03	16.0s
SGM	4.1e-04	3.0e-03	1.2s	2.8e-04	1.4e-03	4.4s	1.1e-04	4.8e-04	16s
Upwind	4.3e-04	9.3e-05	1.0s	2.1e-04	6.0e-05	4.2s	9.4e-05	3.8e-05	14.8s

Table 6. L^2-error (Er.) for flow variables and CPU times produced by the ***second-order FV schemes*** at $t = 2000$s; steady smooth flow over a *non-differentiable* topography.

	***N* = 11 (coarse)**			***N* = 21 (medium)**			***N* = 41 (fine)**		
	Er. *h*	**Er. *q***	**CPU**	**Er. *h***	**Er. *q***	**CPU**	**Er. *h***	**Er. *q***	**CPU**
Etta-SWE	3.6e-04	2.6e-03	3.2s	2.4e-04	1.2e-03	13.0s	8.0e-05	2.8e-04	48.1s

Hydr-Rec	4.4e-03	1.5e-02	3.3s	1.7e-03	5.3e-03	12.0s	7.8e-04	1.7e-03	43.5s
SGM	3.6e-04	2.6e-03	3.8s	2.4e-04	1.2e-03	12.6s	8.0e-05	2.8e-04	45.5s
Upwind	3.8e-04	1.6e-03	3.7s	2.0e-04	3.2e-04	12.8s	8.8e-05	1.1e-04	41.8s
RKDG2	3.6e-04	1.7e-03	16s	1.6e-04	4.0e-04	60s	9.8e-05	2.3e-04	321s

5.2 *Steady smooth flows over a non-differentiable topography*

Similar aspects, as in Subsection 5.1, are studied herein for steady flows over the same spatial 1D domain but with a *non-differentiable* topography (e.g. see within Figure 4). Again, in the first sub-case, the *C*-property is verified numerically for a quiescent flow conditions, defined by $h + z = 12$m and $q = 0$ m^2/s, using the same model configurations, meshes and output time as in the previous test. As displays Table 3, for all the present topography discretizations have led to L^2-errors that are in the range of round-off. Hence, they all seem to (numerically) satisfy the C-property irrespective of the mesh size, the accuracy-order of the numerical scheme and the differentiability property of the topography.

The second sub-case considers a smooth steady subcritical flow where the constant discharge is 8m^2/s and the initial water level is $h + z = 12$m. Inflow discharge and water level at the downstream are imposed as physical boundary conditions, which are completed by transmissive numerical boundary conditions. The same mesh characteristics and output time as before are used and similar series of simulations are undertaken using the first- and second-order models, respectively. The predicted depth and discharge produced by the different topography discretization techniques are compared in Figure 4 and Figure 5, respectively, for the first- and second-order schemes; Table 5 and Table 6 contain the associated L^2-errors that are measured with respect to the analytical solutions. From these tables, it is noteworthy that the Upwind approach maintains the top position as being the best match to the first-order scheme; in this framework, it generates the lowest discharge errors amid any other possible configuration (including with the second-order schemes) and achieves depth errors with similar order of magnitude as for the errors produced by the other techniques that performed best with the second-order schemes (i.e. Tables 5 vs. Table 6). The Etta-SWE and the SGM maintain the same behaviour noted in the previous test; they delivered similar predictions and, again, seem to benefit most from the mesh refinement and the increase to second-order accuracy generating eventually the smallest depth errors overall. The RKDG2 method does not appear to predict the steady discharge with the same level of accuracy as for the case of the *differentiable* topography; yet it provides a close performance to the Upwind, SGM and Etta-SWE approaches with the second-order FV scheme. The Hydr-Rec, in contrast to the others approaches, fails to supply consistent predictions and hence exposes a clear disability in handling steady flow over a *non-differentiable* topography irrespective of the accuracy-order of the FV model, the mesh size and despite the smooth character of the flow.

Consequently, Upwind, RKDG2, SGM, and Etta-SWE are observed to be reliably applicable for flow simulation involving *non-differentiable* topography contrasted with the standard Hydr-Rec, which its validity is questionable, so far.

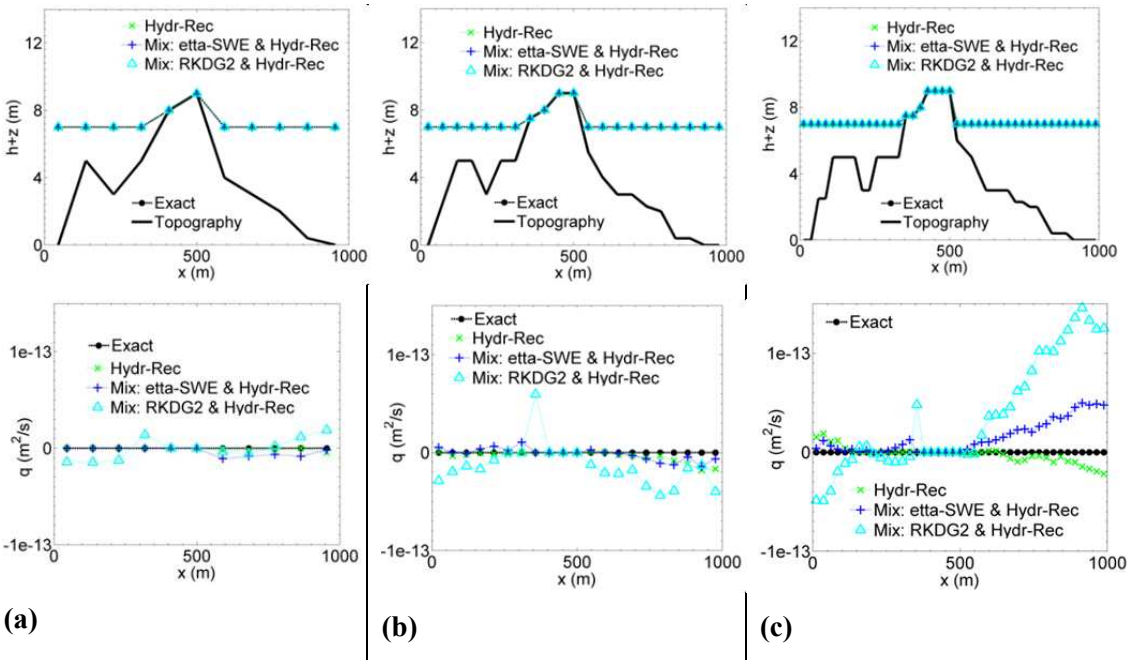

Figure 6. C-property verification in a wet/dry domain involving *non-differentiable* topography; results produced by the ***second-order*** Godunov-type models using a mix-mode with the Hydr-Rec: (a) $N = 11$, (b) $N = 21$, and (c) $N = 41$.

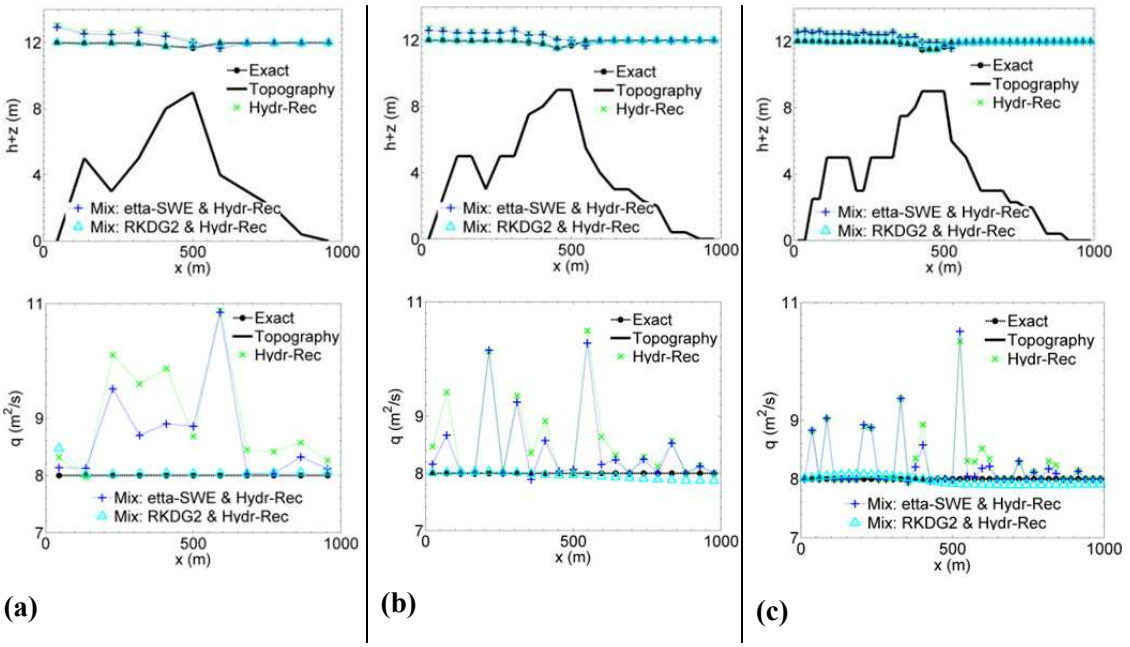

Figure 7. Comparison between the topography discretization approaches reproduced by the ***second-order*** Godunov-type models and in a mix-mode with the Hydr-Rec: (a) $N = 11$, (b) $N = 21$ and (c) $N = 41$.

Table 7. L^2-error for flow variables and CPU times at t = 2000s for the smooth over a *non-differentiable* topography. Mix-mode approaches coupled with the Hydro-Rec within *second-order* accurate Godunov-type models.

	***N* = 11 (coarse)**			***N* = 21 (medium)**			***N* = 41 (fine)**		
	Er. *h*	**Er. *q***	**CPU**	**Er. *h***	**Er. *q***	**CPU**	**Er. *h***	**Er. *q***	**CPU**
Hydr-Rec	4.4e-03	1.5e-02	3.3s	1.7e-03	5.3e-03	12.0s	7.8e-04	1.7e-03	43.5s
Etta-SWE	3.6e-03	1.2e-02	3.9s	1.5e-03	4.6e-03	15.0s	7.3e-04	1.7e-03	55.5s
RKDG2	3.6e-04	1.7e-03	18s	1.6e-04	4.0e-04	66s	9.8e-05	2.3e-04	354s

Finally a third sub-case is introduced to further investigate the Hydr-Rec approach and attempting to gain insight on possible reason(s) for its poor behaviour observed previously. For this purpose, the mix-mode variants Etta-SWE & Hydr-Rec and RKDG2 & Hydr-Rec (see subsection 4.6) are herein considered –taken together with the second-order MUSCL scheme. Their C-property ability of the Hydr-Rec variants is re-checked for a *wet/dry initial condition* (i.e. $h + z$ = 7m and q = 0m^2/s) and they are re-applied to simulate the second sub-case. Figure 6 displays the steady state profiles of the free-surface elevation and the discharge accomplished by the Hydr-Rec alternatives for the wet/dry C-property test, and Figure 7 contains their results for the steady moving water over the *non-differentiable* topography where their associated L^2-Errors are listed in Table 7. As indicate Figure 6, all Hydr-Rec variants maintain the initial free-surface condition after 2000s and reproduce zero discharges; hence are able to balance flux and topography gradients for wet/dry domain with complex topography. On the other hand, when resolving the smooth steady flow over the *non-differentiable* topography (wet domain), the Hydr-Rec variants supply dissimilar results. In effect, the incorporation of the Etta-SWE is found to provide insufficient gain in terms of accuracy, as reflects the depth errors in Table 7 and the discharges prediction displayed in Figure 7. In contrast, the Hydr-Rec & RKDG2 merge supplies conservative predictions without showing any signs of potential instability. These findings hence suggest that the Hydr-Rec and the RKDG2 are supremely compatible for steady flows over *non-differentiable* topographies as well as for the unsteady case as it is demonstrated subsections 5.3 and 5.4.

5.3 *Transient discontinuous flow over steps*

The transient dam-break flow over steps is considered to further explore the topography discretizations configurations, explored in subsection 5.2, for an *unsteady flow* over a *non-differentiable* topography. This test case is featured by different types of water flow

discontinuities and a *large abrupt* change in the topography level at the step (i.e. from 0m to 8m). The spatial domain is [0; 1500m] and the steps are represented by:

$$z(x) = \begin{cases} 8 & \text{if } \left| x - \frac{1500}{2} \right| \le \frac{1500}{8} \\ 0 & \text{otherwise} \end{cases} \tag{23}$$

The initial condition separates two still water levels as described below,

$$h(x,t) = \begin{cases} 20 - z(x) & \text{if } x \le \frac{1500}{2} \\ 15 - z(x) & \text{Otherwise} \end{cases} \tag{24}$$

Transmissive boundary conditions are used for the upstream and the downstream boundary cells. Since no analytical solution is available for this test, alternative simulation results produced by a third order well-balanced RKDG model on a grid with 500 cells are treated as reference solutions (see Figure 8). Simulations are made on three meshes comprising 100, 200 and 400 cells, respectively. The results at t = 16s and t = 61s, i.e. before and after the dam-break wave reaches the 8m gap in the bed level, are collected in Figure 9. The upper panel within Figure 9 presents the zoom-in depth profiles at t = 16s achieved by the Etta-SWE, SGM, Upwind, Hydr-Rec (with the second-order FV scheme), RKDG2, and the two mix-mode variants Etta-SWE & Hydr-Rec, and RKDG2 & Hydr-Rec. At t = 16s, all models delivered fairly similar predictions agreeing closely with the reference solution, namely for the finest mesh where all the predicted depth profiles seem to overlap. For coarser meshes, the RKDG2 approach seems also advantageous for the unsteady case as it delivers a more accurate capture to flow transition than all the FV-based models.

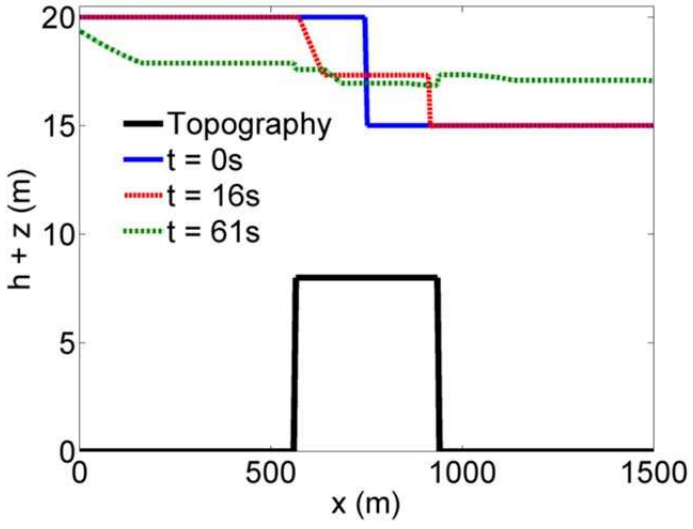

Figure 8. Unsteady dam-break flow profiles over steps at t = 0s, 16s and 61s. Results produced by the RKDG3 model on a fine grid of 500 cells (Kesserwani and Liang 2011).

At t = 61s, the corresponding zoom-in profiles of the water levels are presented in the lower panel within Figure 9. Apart from the FV-based Hydr-Rec variants, all the other models

have closely reproduced the reference solution with the same characteristics as for t = 16s. In this case, however, the anticipated poor behaviour of the FV-based Hydr-Rec variants is seen to expand leading to predictions that dissociate from the others. This further deterioration in performance is suspected to occur due to the comparatively high and sharp variation in the topography gradient at the steps (see next paragraph for the relevant analysis). On the other hand, the RKDG2 & Hydr-Rec variant is observed to succeed, again, in achieving consistent predictions in spite of the unsteadiness of flow and the largeness and sharpness of the topography gradients.

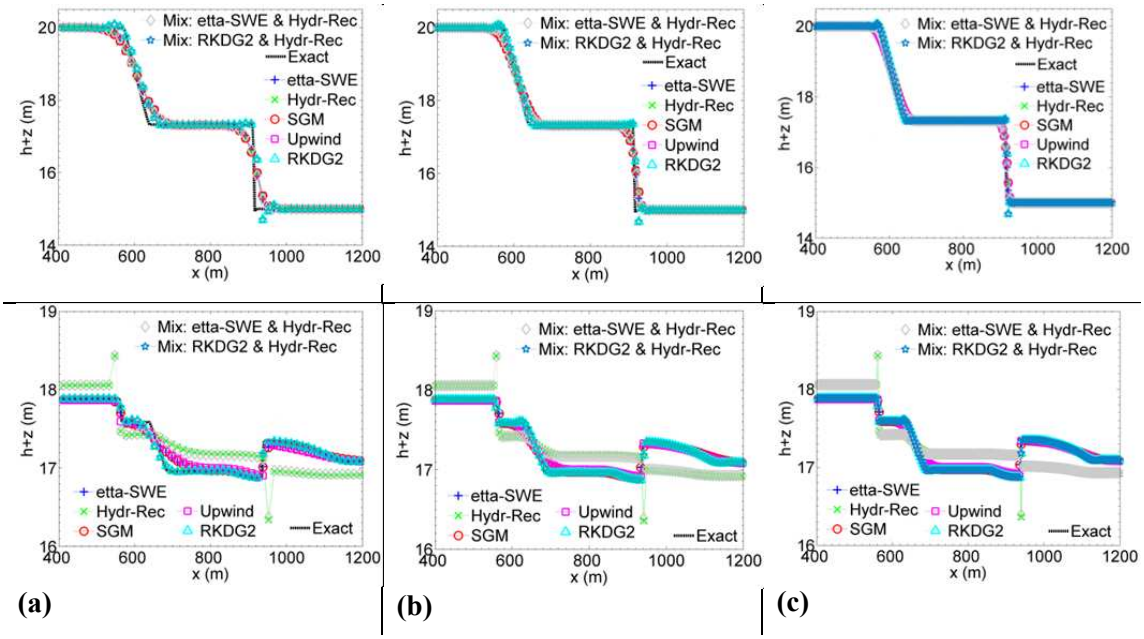

Figure 9. Magnified numerical depth profiles for the unsteady dam-break flow over steps. Upper panel: t = 16s, lower panel t = 61s; row (a) N = 100, row (b) N = 200, and row (c) N = 400.

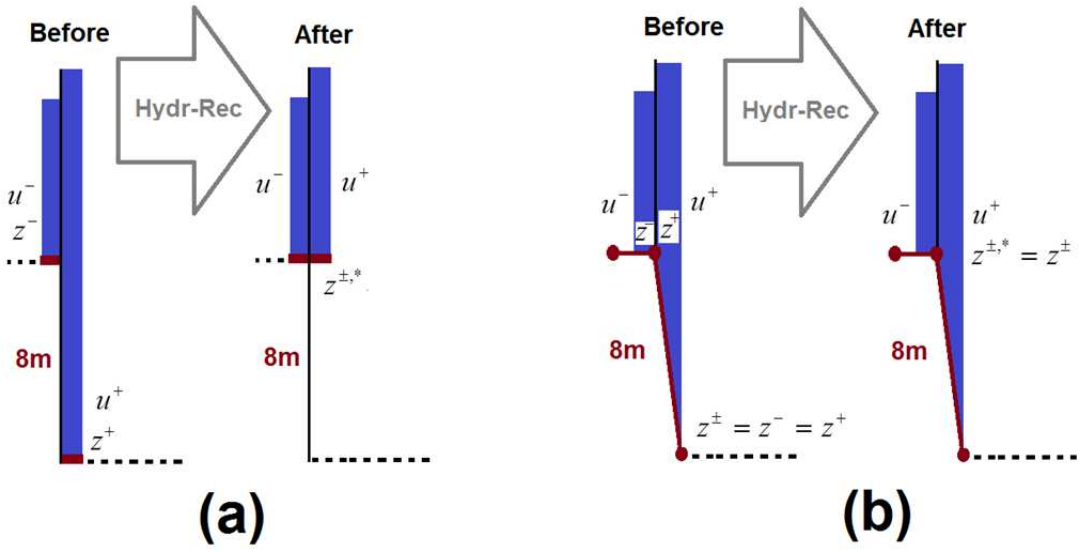

Figure 10. Action of the Hydr-Rec on the interface *topography* and relating to the velocity components (wet case): **(a)** *FV configuration* and **(b)** *RKDG2 configuration*.

Supported by the present and past numerical experiments, it can be argued that the Hydr-Rec approach is radically compatible with the RKDG2 framework. In fact, the underlying reason for this compatibility rests on the *continuity* property provided by the local P^1-projection of z_h within the RKDG2 method, which perfectly helps the Hydr-Rec to avoid any artificial change in the topography, namely when intertwining with wetting and drying. To explain this further, Figure 10 demonstrates the local behaviour of the Hydr-Rec at the second step. As indicate Figure 10(a), the Hydr-Rec particularly records the original velocities u^- and u^+ that are associated with original discontinuous values z^- and z^+, but are required later for use with the new single topography value $z^{\pm,*}$ (i.e. obtained via the maximum; step 3-d in subsection 4.3). Fortunately, the RKDG2 discrete representation to the topography is *continuous* (i.e. $z^+ = z^- = z^{\pm}$) and this property provides the Hydr-Rec *no other option but to retrieve the original interface topography* (i.e. used previously to calculate u^- and u^+). In contrast, with the FV method, the Hydr-Rec must cancel the lower value of the topography z^+, to enforce continuity, and hence incompatibly associate its velocity value u^+ for use with the new value $z^{\pm,*}$, see Figure 10(a). From the analysis, it appears that the performance of FV-based Hydr-Rec variants may be exposed to decrease in proportion with an increase in the height of a topographic step. Supported further by the past numerical experiments, it seems that the RKDG2 method is, by far, the best complement to the Hydr-Rec to obtain a second-order accurate and conservative water wave model for flow simulations with uneven topographies with potential occurrence of wetting and drying.

5.4 *Experimental dam-break flow over a step with wetting and drying*

Another scenario of a breaking wave over a topographic step is assumed to further examine the performance of the Hydr-Rec variants when wetting and drying may occur. The 1D channel configuration is straight with one steep change in the bed level at the middle of channel, where an imaginary dam is initially assumed. The computational domain is [-10m; +10m] in which the bed level downstream of the dam is 0.071m and the height of the step is 0.12m. Upstream of the dam, the initial condition of water level is 0.399m. In a first sub-case, a wet domain is assumed where the initial water level downstream of the dam is 0.075m. In a second sub-case, the level downstream of the dam is 0m assuming that the wave breaks over a dry zone. The Hydr-Rec variants are executed on a mesh with 100 cells. Figure 11 shows the numerical depth profiles reproduced for both sub-cases after 1s and 4s from the dam's removal, together with the experimental depths (Vasquez and Roncal 2009).

In the wet sub-case (Figure 11 – upper panel), the RKDG2 & Hydr-Rec provides the closest agreement with experimental data providing, eventually at t = 4s, improved capture to the shock induced by the step and the smooth zone thereafter than the two FV-based Hydr-Rec variants. The Etta-SWE & Hydr-Rec variant does not appear to function better than the traditional Hydr-Rec, namely at t = 4s in the vicinity of the step where it achieves a poorer capture to flow. However, in this test, the behaviour of the FV-based Hydr-Rec variants remains quite satisfactory, contrasted with the observations in the previous test, and this is likely because of very low height of the step. In the wet/dry sub-case (Figure 11 – lower panel) all the Hydr-Rec variants are observed to perform globally well suggesting that the Hydr-Rec approach is functional as a wetting and drying condition within both the FV and the RKDG2 schemes. Nonetheless, taken as whole, the RKDG2 & Hydr-Rec merge is likely to be favoured as the best alternative for multipurpose shallow water flow simulations as it does not particularly risk collapsing in the wet cases in spite of the complexity of the flow and the non-differentiability of the topography.

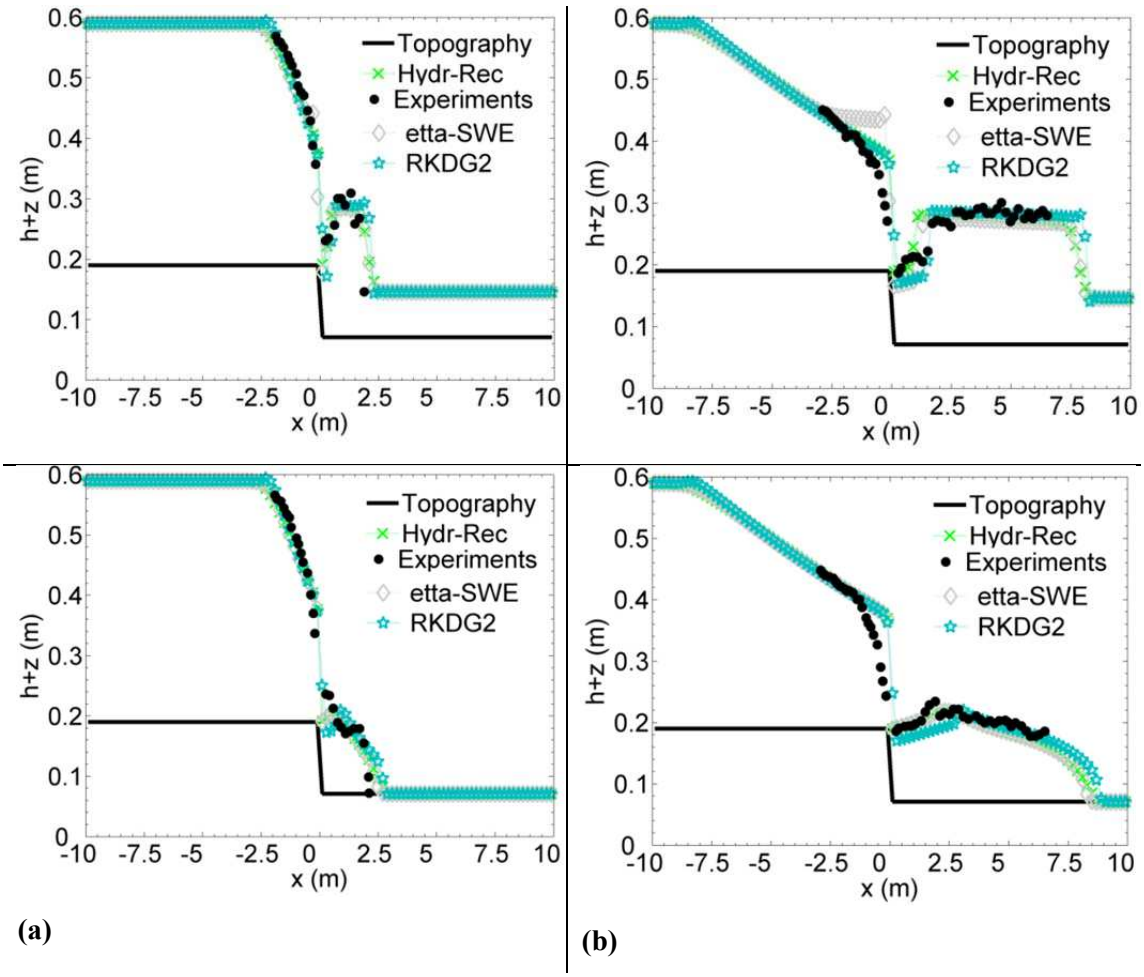

Figure 11. Experimental dam-break over a step; numerical depth profiles produced by the ***second-order*** Godunov-type schemes incorporating Hydro-Rec. Upper panel: wet case, lower panel: wet/dry case, row (a) t = 1s, and row (b) t = 4s.

6. Summary, discussions and conclusions

This work has presented, assessed and compared several topography discretization techniques relevant to Godunov-type shallow water numerical models. Five different discretization approaches that satisfy the C-property, i.e. theoretically valid for lake at rest hypotheses, have been considered and their ability to resolve more complicated flows over topography has been thoroughly explored. Of these approaches, four are attributed to the FV formulation (up to second-order via MUSCL interpolation) in which the topography is locally represented as piecewise-constant with discontinuities at interfaces; whereas the fifth approach is particular to RKDG2 method (second-order) that locally integrates the topography as piecewise-linear. The five approaches have been reviewed in their basic form together with alternative mix-mode forms; they have effectively consisted of:

- The Upwind approach that locally decomposes, i.e. at interfaces, the topography source term via the projection onto the linearized characteristic basis and thereby discretizes the topography gradient term in harmony with the local upwinding of the flux.
- The SGM that uses a cell-centred pointwise approximation to the topography gradient. It first reconstructs free-surface variable at interfaces (i.e. sum of actual depth components and topography values) and then redefines equivalent Riemann states associated to a locally-continuous topography at interface (i.e. averaged).
- The Etta-SWE in which the underlying mathematical form of the SWE incorporates the free-surface component as a main variable. Technically, the Etta-SWE acts on flux and topography similar to the SGM.
- The Hydr-Rec approach that lies on a depth-positivity-preserving condition to locally redefine the flux and source term, at interfaces, while satisfying the C-property. It first maintains the original velocities relative to discontinuous states of the discrete topography at interfaces. Afterwards, it imposes locally-continuous topography at interfaces (takes the maximum values) and accordingly redefines new depth components that preserve positivity. Finally, it employs Riemann states relevant to the positivity-preserving depth components and incorporating the original velocities to calculate flux, at interfaces, and discretizes the topography gradient as local pointwise.
- The RKDG2 method that rests on a projection to the topography onto the local basis of first-order polynomial. The topography projection is continuous, including at the interfaces, and genuinely integrates the gradient term by a local pointwise manner.
- Mix-mode approaches related to the Hydr-Rec, i.e. Etta-SWE & Hydr-Rec and RKDG2 & Hydr-Rec. These approaches have been aimed to examine the effect of wetting and

drying condition, particular to the Hydr-Rec, on pertinent topography discretization techniques and to ultimately provide an improved variant to the traditional Hydr-Rec.

The topography discretization approaches have been evaluated for a selection of hydraulic tests with uneven topographies that includes steady flows – covering the stationary case and cases with non-zero velocities incorporating smooth, gradual and/or rapid variations in the flow regime – and unsteady highly-perturbed flows. Qualitative comparisons among the approaches and against reference data (i.e. analytical solution, alternative simulations, or experiments) have been illustrated with particular analyses in relation to the issue of differentiability of the topography, the density of the mesh, the effect of wetting and drying (when applicable), and the impact of the accuracy-order (for the FV-based approaches). For the analytical steady tests, runtime costs and L^2-errors have been recorded and used as a quantitative means to refine the performance analysis among the approaches.

The numerical experiments confirm that all the candidates are unconditionally valid for the C-property – despite the mesh size and the accuracy-order of the numerical formulation – and conclude that the differentiability property of the topography is the most notable factor that may affect their behaviour in the simulation of steady and unsteady dynamic flows.

- For a differentiable topography, all the discretization techniques are experienced to operate well for a reasonably fine mesh and despite the presence of compound flow transitions. With the first-order FV scheme, Upwind outperforms and Hydr-Rec may be positioned as second best for being comparatively fit on coarse meshes, whereas Etta-SWE and SGM only reach a comparable performance to the others when the mesh is refined. However, this standing is seen to change when the FV-based discretization techniques are integrated in the context of a second-order MUSCL scheme; Etta-SWE and SGM show to benefit most from the mesh refinement and ultimately present the top performance whereas the functioning of Upwind and Hydr-Rec drop dramatically irrespective of the mesh density – the former namely notes local improvement at smooth flow zones (i.e. subcritical) whereas the latter does not improve in any respect. Nevertheless, for a differentiable topography, RKDG2 places ahead of all the FV-based performers achieving the most accurate and conservative predictions – specifically for very coarse mesh it also achieves comparable runtime.
- For a non-differentiable topography, the traditional Hydr-Rec seems to be at risk of falling short contrasted with Upwind, Etta-SWE, SGM and RKDG2 that could somewhat attain the expected behaviour. In steady smooth flow, Upwind again excels with the first-order scheme reaching unbeatable prediction for the discharge; with the second-order MUSCL scheme, Upwind notes minor degeneration in terms of discharge predictions but

remains leading with the second-order models. Etta-SWE and SGM reveal, again, a rational responsiveness to ameliorate with both mesh refinement and increase of accuracy-order, where they ultimately accomplish the most accurate resolution to the water depth. RKDG2 achieves second best in the prediction of the discharge, and best in the predictions of the water depth on the coarse meshes where it nearly matches the performance of Upwind with reasonable computational cost. The traditional Etta-SWE, SGM, Upwind and RKDG2 are also experienced to maintain stable in reproducing unsteady dam-break flows over non-differentiable topography where the candidates achieve consistent predictions on fine mesh and with the second-order accurate schemes; however, in this case, RKDG2 overtops the FV-based techniques in terms of providing a finer capture to the flow transients on a relatively coarse mesh.

- The traditional Hydr-Rec is able to correctly incorporate both wetting and drying and the topography while satisfying the C-property. However, as opposed to the other candidates, it appears to have a knock-on effect when applied to reproduce moving water flows over non-differentiable topographies, which may impact its reliability. The merge Etta-SWE & Hydr-Rec does little improvement over the traditional Hydr-Rec and remain exposed to the same side effect as with the traditional Hydr-Rec. In contrast, the merge RKDG2 & Hydr-Rec does not show any sign of inconsistencies; it exactly maintains the behaviour of the traditional RKDG2 for wet domains, effectively uses the Hydr-Rec for modelling moving wet/dry fronts, and works unfailingly in any case, i.e. despite the differentiability of the topography and/or the complexity of flow. Analysis to the functioning of both approaches suggests that RKDG2's discretization to the topography suits the operation of the Hydr-Rec so as to genuinely undergo wetting and drying without compromising the (original) discretization of the topography.

To sum up, this study comes out with: (a) Upwind as the best complement to a first-order Godunov-type scheme; (b) SGM, or alternatively Etta-SWE, as being mostly effective with the second-order MUSCL scheme; (c) RKDG2 as being highly suited for coarse mesh simulations; (d) Hydr-Rec as being able to better serve as a wetting and drying condition rather than a topography discretization approach, and to particularly fit the RKDG2 framework to provide an accurate, conservative and sustainable shallow water numerical model for all-purposes simulations.

Notation

x = space coordinate [m]

t = time coordinate [m]

h = water depth [m]

q = flow discharge per unit width [m^2/s]

z = topography [m]

u = velocity [m/s]

η = free-surface elevation [m]

c = wave celerity [m/s]

g = acceleration due to gravity [m^2/s]

$\mathbf{U}$ = vector of the conserved quantities [-]

$\mathbf{F}$ = spatial flux vector [-]

$\mathbf{S}$ = vector containing the source term

$\mathbf{J}$ = Jacobien matrix of the flux vector with respect to the flow vector

$\lambda^{1,2}$ = real eigenvalues of $\mathbf{J}$

$\mathbf{e}^{1,2}$ = real eigenvectors proper to the real eigenvalues $\lambda^{1,2}$

N = number of computational cells

I_i = computational cell

$x_{i+1/2}$ = interface point separating adjacent cells I_i and I_{i+1}

x_i = centre of cell I_i

Δx = length of a cell I_i

$\mathbf{U_h}|_{I_i}$ = local approximate solution at cell I_i

$\mathbf{S_h}|_{I_i}$ = local approximation to $\mathbf{S}$ at cell I_i

$\mathbf{F}|_{I_i}$ = local approximation to $\mathbf{F}$ at cell I_i

$z_h|_{I_i}$ = local topography approximation at cell I_i

$\tilde{\mathbf{F}}_{i+1/2}$ = numerical flux at $x_{i+1/2}$

$\alpha_{i+1/2}^{1,2}$ = wave strengths relative to the Roe Riemann problem solution at $x_{i+1/2}$

$\tilde{\lambda}_{i+1/2}^{1,2}$ = eigenvalues relative to the Roe Riemann problem solution at $x_{i+1/2}$

$\tilde{\mathbf{e}}_{i+1/2}^{1,2}$ = eigenvectors relative to the Roe Riemann problem solution at $x_{i+1/2}$

I = identity matrix

$\tilde{J}_{i+1/2}$ = approximate linearized Jacobian at $x_{i+1/2}$ due to the Roe Riemann solver

$\mathbf{R}_{i+1/2}$ = matrix containing the eigenvectors $\tilde{\mathbf{e}}_{i+1/2}^{1,2}$

$\varepsilon_{i+1/2}^{1,2}$ = threshold limits for the entropy fix to the Roe Riemann problem solution at $x_{i+1/2}$

$\mathbf{U}^{-}_{i+1/2} = \mathbf{U}_{\mathbf{h}}|_{I_i}(x^{-}_{i+1/2})$ = left limit of the approximate solution at $x_{i+1/2}$

$\mathbf{U}^{+}_{i+1/2} = \mathbf{U}_{\mathbf{h}}|_{I_{i+1}}(x^{+}_{i+1/2})$ = right limit of the approximate solution at $x_{i+1/2}$

$\nabla_i(\mathbf{U}_{\mathbf{h}})$ = slope limited gradient term relative to the MUSCL at cell I_i

$\boldsymbol{\varphi}$ = slope limiter function

$\mathbf{U}^{0,1}_i(t)$ = local finite element coefficients of the flow vector at cell I_i

$z^{0,1}_i$ = local finite element coefficients of the topography function at cell I_i

$\mathbf{L}^{0,1}_i$ = spatial DG2 operators relative to the update of the coefficients $\mathbf{U}^{0,1}_i(t)$

$\eta^{-}_{i+1/2}$ = left limit of the free-surface elevation at $x_{i+1/2}$

$\eta^{+}_{i+1/2}$ = right limit of the free-surface elevation at $x_{i+1/2}$

$z^{-}_{i+1/2}$ = left limit of the topography at $x_{i+1/2}$

$z^{+}_{i+1/2}$ = right limit of the topography at $x_{i+1/2}$

$z^{\pm}_{i+1/2}$ = single topography value at $x_{i+1/2}$ (within Etta-SWE and SGM)

$\overline{h}$ = averaged water depth for source term evaluation at cell I_i

$\overline{\eta}$ = averaged free-surface for source term evaluation at cell I_i (within Etta-SWE)

$\partial_x z$ = approximation to the topography gradient at cell I_i

$z^{+,*}_{i+1/2}$ = numerical left limit of the topography, i.e. $h^{K}_{i+1/2} = \eta^{K}_{i+1/2} - z^{K}_{i+1/2}$ (K = +,-)

$z^{\pm,*}_{i+1/2}$ = single topography value at $x_{i+1/2}$ defined by the maximum (within Hydr-Rec)

References

Audusse, E., Bouchut, F., Bristeau, M.O., Klein, R., Perthame, B. (2004). A fast and stable well-balanced scheme with hydrostatic reconstruction for shallow water flows. *SIAM J. Sci. Comput.* 25, 2050–2065.

Bermúdez, A., Vázquez-Cendón, M.E. (1994). Upwind methods for hyperbolic conservation laws with source terms. *Comput. Fluids* 23, 1049–1071.

Cockburn, B., Shu, C.W. (2001). Runge–Kutta discontinuous Galerkin methods for convection-dominated problems. *J. Sci. Comput.* 16, 173–261.

Crnjaric-Zic, N., Vukovic, S., Sopta, L. (2004). Balanced finite volume WENO and central WENO schemes for the shallow water and the open-channel flow equations. *J. Comput. Phys.* 200, 512–548.

Delis, A.I. and Kampanis, N.A. (2009). Numerical flood simulation by depth averaged free surface flow models. In: Achim Sydow (Ed.), E*nvironmental Systems, Encyclopedia of Life Support Systems* (EOLSS), Oxford, UK.

García-Navarro, P., Vázquez-Cendón M.E. (2000). On numerical treatment of the source terms in shallow water equations. *Comput. Fluids* 29, 951–979.

George, DL. (2008). Augmented Riemann solvers for the shallow water equations over variable topography with steady states and inundation. *J. Comput. Phys.* 227, 3089–3313.

Godunov, S. K. (1959). A Difference scheme for numerical solution of discontinuous solution of hydrodynamic equations. *Math. Sbornik* 47, 271–306.

Greenberg, J.M., LeRoux, A.Y. (1996). A well-balanced scheme for numerical processing of source terms in hyperbolic equations. *SIAM J. Numer. Anal.* 33, 1–16.

Guinot, V. (2003). *Godunov-type schemes: An introduction for engineers.* Elsevier: Amsterdam.

Kesserwani, G., Liang, Q. (2011). A conservative high-order discontinuous Galerkin method for the shallow water equations with arbitrary topography. *Int. J. Numer. Meth. Eng.* 82, 47–67.

Kesserwani, G., Liang, Q. Locally limited and fully conserved RKDG2 shallow water solutions with wetting and drying. *J. Sci. Comput.* 50, 120–144.

Kesserwani, G., Liang, Q., Vazquez, J, and Mosé R. Well-balancing issues related to the RKDG2 scheme for the shallow water equations. *Int. J. Numer. Meth. Fluids* 2010; 62,

428–448.

Krivodonova, L., Xin, J., Remacle, J.F., Chevaugeon, N., Flaherty, J.E. (2004) Shock detection and limiting with discontinuous Galerkin methods for hyperbolic conservation laws. *App. Numer. Math.* 48, 323–338.

LeFloch, P.G., Tanh M.D. (2012). A Godunov-type method for the shallow water equations with discontinuous topography in the resonant regime. *J. Comput. Phys.* 230, 7631–7660.

LeVeque, R.J. (1998). Balancing source terms and flux gradients in high resolution Godunov methods. *J. Comput. Phys.* 146, 346–365.

Lhomme, J., Gutierrez-Andres, J., Weisgerber, A., Davison, M., Mulet-Marti, M., Cooper, A., Gouldby, B. (2010). Testing a new two-dimensional flood modelling system: analytical tests and application to a flood event. *J. Flood Risk Management* 3, 33–51.

Liang, Q. (2010). Flood simulation using a well-balanced shallow flow model. *J. Hydraulic. Eng.* 136, 669–675.

Liang, Q., Borthwick, A.G.L. (2009). Adaptive quadtree simulation of shallow flows with wet-dry fronts over complex topography. *Comput. Fluids* 38, 221–234.

Murillo, J., Garcia-Navarro, P. (2010). Weak solutions for partial differential equations with source terms: Application to the shallow water equations. *J. Comput. Phys.* 229, 4327–4368.

Murillo, J., Garcia-Navarro, P. (2012).Wave Riemann description of friction terms in unsteady shallow flows: Application to water and mud/debris floods. *J. Comput. Phys.* 231, 1963–2001.

Néelz, S. Pender, G. (2010). *Benchmarking of 2D hydraulic modelling packages*. UK Environment Agency, Science Project Number: SC080035/R2.

Noelle, S., Pankratz, N., Puppo, G., Natvig, J.R. (2006). Well-balanced finite volume schemes of arbitrary order of accuracy for shallow water flows. *J. Comput. Phys.* 213, 474–499.

Nujic, M. (1995). Efficient implementation of non-oscillatory schemes for the computation of free-surface flows. *J. Hydr. Res.* 33, 101–111.

Roe, P.L. (1981). Approximate Riemann solvers, parameter vectors and difference schemes. *J. Comput. Phys.* 43, 357–372.

Rogers, B.D., Borthwick, A.G.L., Taylor, P.H. (2003). Mathematical balancing of flux gradient and source terms prior to using Roe's approximate Riemann solver. *J. Comput.*

Phys. 192, 422–451.

Toro E.F. (2001). Shock-capturing methods for free-surface shallow flows. Wiley: New York.

Toro, E.F., García-Navarro, P. (2007). Godunov-type methods for free-surface shallow flows: a review. *J. Hydr. Res.* 45, 737–751.

van Leer, B. (1979). Towards the Ultimate Conservative Difference Scheme, V. A Second Order Sequel to Godunov's Method. *J. Comput. Phys.* 32, 101–136.

Vazquez, J.A., Roncal J.J. (2009). Testing River2D and Flow-3D for sudden dam-break flow simulation. Proc. *Canadian Dam Association Annual Conference*, Canada.

Vázquez-Cendón, M.E. (1999). Improved treatment of source terms in upwind schemes for the shallow water equations in channels with irregular geometry. *J. Comput. Phys.* 48, 497–526.

Vukovic, S., Sopta, L. (2002). ENO and WENO schemes with the exact conservation property for one-dimensional shallow water equations. *J. Comput. Phys.* 179, 593–621.

Wang, Y., Liang, Q., Kesserwani, G., Hall, J.W. A 2D shallow flow model for practical dam-break simualtions. *J. Hydraulic Res.* 49, 307-316.

Xing, Y., Shu, C.W. (2006). A new approach of high order well-balanced finite volume WENO schemes and discontinuous Galerkin methods for a class of hyperbolic systems with source terms. *Commun. Comput. Phys.* 1, 101–135.

Zhou. J.G., Causon, D.M., Ingram, D.M., Mingham, C.G. (2001). The surface gradient method for the treatment of source terms in the shallow-water equations. *J. Comput. Phys.* 168, 1–25.